Deciphering the geochemistry of two key Paleoproterozoic siliciclastic sequences of the Piedra Alta Terrane (Río de la Plata Craton, Uruguay)

Decifrando la geoquímica de dos secuencias paleoproterozoicas siliciclásticas claves del Terreno Piedra Alta (Cratón del Río de la Plata, Uruguay)

Decifrando a geoquímica de duas sequências siliciclásticas paleoproterozóicas chave da Piedra Alta Terrane (Cráton Río de la Plata, Uruguai)

Blanco, Gonzalo; Abre, Paulina; Lanfranchini, Mabel; Cingolani, Carlos A.; Ferrizo, Hector; Piñeyro, Daniel; Uriz, Norberto J.; Benítez, Manuela E.

Gonzalo Blanco
gblanco@cure.edu.uy
Universidad de la República, Uruguay

Paulina Abre
Universidad de la República, Uruguay

Mabel Lanfranchini
Universidad Nacional de La Plata, Argentina

Carlos A. Cingolani
Universidad Nacional de La Plata, Argentina

Hector Ferrizo
Universidad de la República, Uruguay

Daniel Piñeyro
Universidad de la República, Uruguay

Norberto J. Uriz
Universidad Nacional de La Plata, Argentina

Manuela E. Benítez
Universidad Nacional de La Plata, Argentina

Agrociencia Uruguay
Universidad de la República, Uruguay
ISSN-e: 2730-5066
Periodicity: Bianual
vol. 26, no. 1, Esp., e525, 2022
agrociencia@fagro.edu.uy

Received: 29 January 2021
Accepted: 27 July 2021
Published: 27 May 2022

URL: http://portal.amelica.org/ameli/journal/506/5064091005/

DOI: https://doi.org/10.31285/AGRO.26.525

Abstract: The geochemistry of two metavolcano-sedimentary sequences deposited in the Piedra Alta Terrane is compared, and their geotectonic evolution is discussed. The Ojosmín Unit (OU) comprises MORB-like basic rocks at the base and a fine-grained siliciclastic sequence interpreted as marine turbidites towards the top. The succession was later obducted during the Orosirian. Whole-rock geochemistry of the metasedimentary rocks of the OU indicates the lack of source rock alteration during deposition (Chemical Index of Alteration, CIA ca. 40-53), implying ice-house climatic conditions in correlation with the worldwide Rhyacian glaciations. Recycling of zircon fractionates the Rare Earth Elements (REE) increasing the amount of HREE, Y, and Hf. Variation ranges of Th/Sc (0.4-4.9), Zr/Sc (30-410), Th/U (2.5-4.3), and of the Eu/Eu * negative anomaly (0.4-0.7) approximate Upper Continental Crust (UCC) values. A new clastic metasedimentary, gently folded unit, the Cerro de la Figurita Formation (CFFm), is erected. The CFFm clastic sedimentation (3,000 m in thickness) represents a deepening upward sequence, starting with polymictic conglomerates deposited in an alluvial fan-dominated environment that evolves to marine turbidites. The CFFm is probably related to a foreland geotectonic setting developed during the Orosirian. The geochemistry of the CFFm reveals similarities to unrecycled UCC, and weathering of the source rocks increases up section (CIA 45-92). Low ratios of Th/Sc (0.3-1.5), Zr/Sc (6-20), Th/U (3-6), high Cr/V (1.1-12.2), and a less pronounced Eu/Eu* negative anomaly of certain samples (0.5-0.9) suggest a contribution from mafic source rocks (probably ophiolitic).

Keywords: geochemistry, provenance, Ojosmín, Cerro Figurita, paleoproterozoic.

Corresponding author: gblanco@cure.edu.uy

Resumen: Se comparan las características geoquímicas de dos secuencias metavolcano-sedimentarias depositadas en el Terreno Piedra Alta y se discute la evolución geotectónica. La Unidad Ojosmín (OU) está compuesta por rocas básicas tipo MORB en la base y una secuencia siliciclástica de grano fino interpretada como turbiditas marinas hacia el tope de la unidad y posteriormente obductadas durante el Orosiriano. La geoquímica en roca total de las rocas metasedimentarias de la OU muestra la ausencia de alteración de la roca madre por meteorización (Índice de Alteración Química, CIA, 40-53) durante la depositación, lo que indica condiciones climáticas del tipo *ice-house* y se correlaciona con las glaciaciones Rhyácicas a nivel mundial. Debido al reciclaje de circón existe un fraccionamiento de las tierras raras (REE), aumentando la cantidad de HREE, Y y Hf. Los rangos de variación de Th/Sc (0,4-4,9), Zr/Sc (30-410), Th/U (2,5-4,3) y la anomalía negativa de Eu/Eu * (0,4-0,7) tienen valores similares a los de la corteza continental superior (UCC). Se define una nueva unidad clástica metasedimentaria que se encuentra plegada en un amplio sinclinal, denominada Formación Cerro de la Figurita (CFFm). La CFFm representa una sedimentación clástica (3.000 m de espesor) grano y estrato decreciente dominada por paquetes de conglomerados polimícticos depositados en un ambiente de abanicos aluviales que evolucionan a condiciones marinas, dominado por turbiditas y depositada en una cuenca de antepaís desarrollada durante el Orosiriano. La geoquímica de CFFm revela similitudes con la UCC no reciclada, y aumento de la alteración de la roca fuente hacia el tope de la secuencia (CIA 45-92). La contribución de rocas fuente máficas (probablemente ofiolíticas) se revela por las bajas relaciones de Th/Sc (0,3-1,5), Zr/Sc (6-20), Th/U (3-6), alto Cr/V (1,1 -12,2) y anomalía negativa de Eu/Eu * menos pronunciada en algunas muestras (0,5-0,9).

Palabras clave: geoquímica, proveniencia, Ojosmín, Cerro Figurita, paleoproterozoico.

Resumo: A geoquímica de duas sequências metavulcano-sedimentares depositadas no terreno Piedra Alta é comparada e a evolução geotectônica é discutida. A Unidade Ojosmín (OU) é composta por MORB como rochas básicas no fundo e sequência siliciclástica de granulação fina interpretada como turbiditos marinhos em direção ao topo e posteriormente obduzidos durante o Orosirian. Toda a geoquímica das rochas metassedimentares OU mostra a ausência da alteração da rocha geradora por intemperismo (Indice de Alteração Química, CIA, 40-53) durante a deposição, indicando as condições climáticas da Ice-house e correlacionadas com as glaciações Rhyacian em todo o mundo. A reciclagem do zircão fraciona as terras raras (REE) aumentando a quantidade de HREE, Y e Hf. A variação de Th/Sc (0.4-4.9), Zr/Sc (30-410), Th/U (2.5-4.3) e a anomalia Eu/Eu* (0,4-0,7) são semelhantes à Crosta Continental Superior (UCC). Uma nova unidade metassedimentar clástica dobrada em amplo sinclinal, chamada Formação Cerro de la Figurita (CFFm.) é definida. O CFFm. sedimentação clástica (3.000 m de espessura) representa uma sequência ascendente de aprofundamento de conglomerados polimíticos depositados em um ambiente dominado por fendas aluviais que evoluem para condições marinhas, dominadas por turbiditos e provavelmente relacionadas a um cenário geotectónico de antepais desenvolvido durante o Orosiriano. A geoquímica da CFFm. mostra um comportamento semelhante com a UCC não reciclada, aumentando o intemperismo da rocha fonte para o topo (CIA 45-92). A contribuição de uma fonte de rochas máficas (provavelmente ofiolítica) é revelada pelas baixas razões de Th/Sc (0.3-1.5), Zr/Sc (6-20), Th/U (3-6), Cr/V alto (1,1 -12,2) e a anomalia negativa Eu/Eu * de algumas amostras (0,5-0,9).

Palavras-chave: geoquímica, proveniencia, Ojosmín, Cerro Figurita, paleoproterozoico.

1. Introduction and geological background

Cratons are continental blocks that preserve the oldest and most varied rocks that have existed throughout the history of the Earth and, therefore, they are key pieces to understand the processes that have formed the current configuration of our planet. The Río de la Plata Craton covers part of southern Brazil, Paraguay, Uruguay, and the central-eastern sector of Argentina, and is subdivided into several terranes or blocks[1][2][3][4][5][6][7][8][9][10] (Figure 1). To the north, the Río de la Plata Craton borders the southern Amazon Craton (Bolivia and Brazil); whereas to the east it borders the allochthonous Cuchilla Dionisio Terrane, which displays a similar age range to the western edge of the Kalahari Craton, and is suspected to have been separated from it before the Brasilian orogeny[11][12][13][14]. To the west, the Río de la Plata Craton is bounded by the Pampia Terrane. The southern limit is marked by the Sierra de la Ventana fold belt, which is not part of the Río de la Plata Craton according to several geochronological studies[15][16][17].

The objective of sedimentary provenance studies is to interpret the history of sedimentary contribution from the erosion of a source rock to the final detritus deposition, allowing us to make paleogeographic reconstructions recognizing the lithogeochemical characteristics of the source rocks[18][19][20]. Source rocks and sedimentary basins)(do not remain stable for long periods, and under ideal circumstances certain characteristics such as changes in the supply areas, drainage network, climate, tectonic environment, and paleoland scape can be recognized and identified to understand the geochemical evolution of the upper continental crust[21]. Therefore, sedimentary provenance studies of these metasedimentary units of the Río de la Plata Craton based on geochemistry provide relevant data to gain insights into the understanding of the evolution of the continental crust and the sedimentary history, from source to sink, of Paleoproterozoic units of Uruguay. In this study, we compare geochemical data of metasedimentary rocks cropping out at two poorly studied sectors of the Piedra Alta Terrane: the Ojosmín area, and the easternmost outcrops of the San José Belt (Fig. 1)

Author notes

gblanco@cure.edu.uy

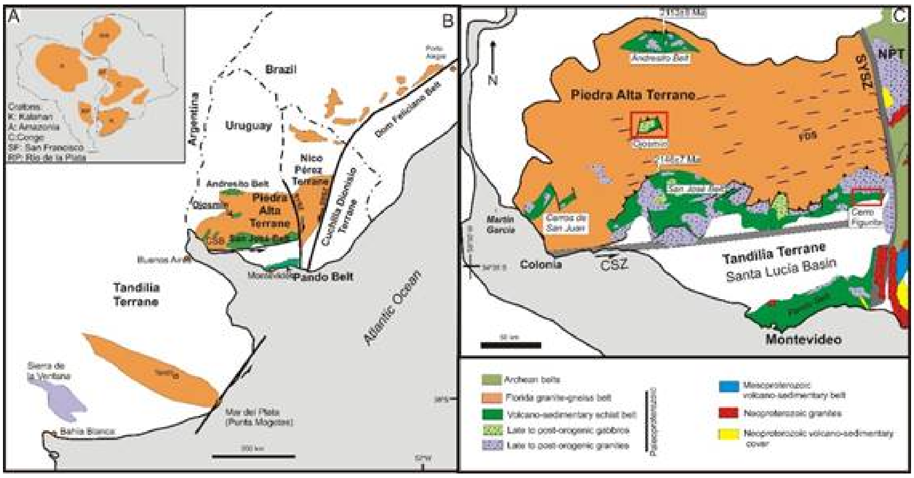

FIGURE 1
A: Location of the Río de la Plata Craton. B: and C: Piedra Alta Terrane in Uruguay Bossi and Cingolani(3). CSZ: Colonia Shear Zone, NPT: Nico Pérez Terrane, FDS: Florida Dike Swarm, SYSZ: Sarandí del Yí Shear Zone

1.1 Piedra Alta and Tandilia Terranes

The Piedra Alta Terrane is constituted by supracrustal belts striking approximately east-west, separated from each other by extensive areas of granites, gneisses, and migmatites grouped into the Florida Belt (Fig. 1)(6)(7)(22)(23)(24). The low-grade San José and Andresito Belts are included within the Piedra Alta Terrane, whereas according to Bossi and Cingolani(3), the medium-grade Pando Belt is part of the Tandilia Terrane, which extends to the south of the Buenos Aires Province in Argentina and is separated from the Piedra Alta Terrane by the Colonia Shear Zone(10)(25). Siliciclastic rocks occur in the supracrustal belts, in volcano-sedimentary units known as the Arroyo Grande Formation (Andresito Belt), Paso Severino Formation (San José Belt), and Montevideo Formation (Pando Belt). While in the Piedra Alta Terrane they are intruded by calc-alkaline, late to post-orogenic granites between 2.05 and 2.09 Ga, in the Tandilia Terrane anorogenic granites show similar crystallization ages (Fig. 2)(26)(27)(28). Geochronological data presented by Santos and others(5) suggest a complex geotectonic scenario for the Piedra Alta-Tandilia Terranes indicating different magmatic events spanning from the Rhyacian to the Stenian period.

A different tectonic evolution characterized the volcano-sedimentary records of the Paso Severino and Arroyo Grande formations(7). The Paso Severino Formation is dominated by marine facies composed of metapelites with intercalated metabasalts and carbonates at the top. The Arroyo Grande Formation is dominated by a thick package of feldspathic metarenites with well-preserved sedimentary structures and interlayered mafic rocks towards the top(29).

The Ojosmín Unit is one of the less-studied areas of the Uruguayan Precambrian Shield, that probably represents a metamorphosed ophiolitic fragment composed of ultramafic, mafic, and metasedimentary rocks intruded by granophyre and trachyte(29). Geological proxies poorly constrain the depositional age at ca. 2.0-2.1 Ga and the tectonic thrusting at ca. 1.9 Ga(29).

In the easternmost area of the San José Belt, at the Cerro Figurita, the metasedimentary rocks comprise coarse polymictic conglomerates, interbedded with volcanoclastic conglomerate at the base, feldspathic arenites at the middle of the sequence, and pelites and wackes resembling turbidites at the top of the section(30). Thus, the lithostratigraphy of the Cerro Figurita is markedly different to that of the Paso Severino

Formation, and the Nd isotope data presented here suggest deposition before 2.0 Ga[30], implying that the unit is younger than the Paso Severino Formation.

Therefore, a new stratigraphic unit called Cerro Figurita Formation (CFFm) is erected in this work and described in detail later (see below).

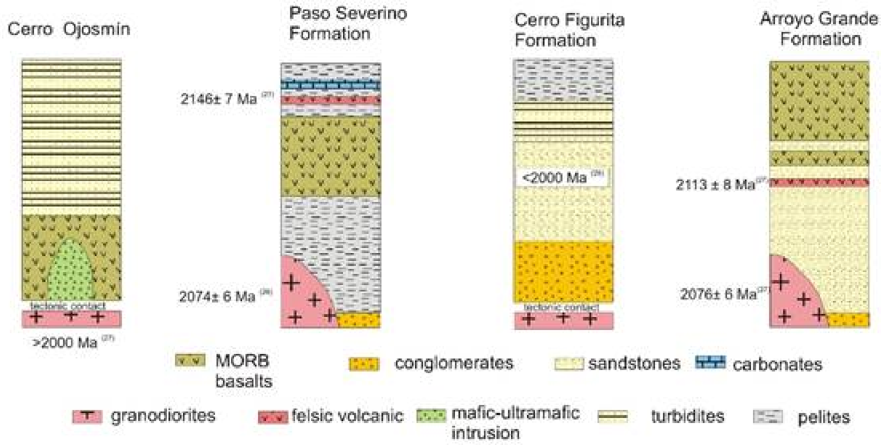

FIGURE 2
Comparison between key meta(volcanic)sedimentary sequence of the Piedra Alta Terrane and their main stratigraphic features from Bossi & Piñeyro[29] and Blanco and others[30]

2. Materials and methods

In order to understand the stratigraphy and the structural geology of both areas, geological maps at 1:20.000 scale and stratigraphic columns were elaborated based on outcrop descriptions and photointerpretation. Standard thin sections of the samples were analyzed using a Leica DM-2500 petrographic microscope at CURE (Treinta y Tres, Uruguay). For geochemical analyses, the samples were pulverized using a jaw crusher and a Cr-steel mill at the Laboratory of Geology (CURE). Geochemical analyses were carried out for 27 samples at Bureau Veritas Minerals Laboratories (Canada). Following lithium borate fusion preparation, major elements and Ni, Zn, Cu, Cr, and Sc were determined by ICP-ES, whereas all other trace elements (including rare earth elements) were measured by ICP-MS. Lower limits of detection (lld) are 0.01% for all major elements except Fe_2O_3, which is 0.04; lld of 0.1 ppm for Nb, Rb, U, Ta, Hf, Y, Zr, Cs, La and Ce; lld of 1 ppm for Ba and Sc; lld of 0.5 ppm for Sr and Ga; lld of 0.2 ppm for Co and Th; 8 ppm for V and Cr and 20 ppm for Ni. Lld of 0.02 ppm for Pr, Eu, and Ho; of 0.3 ppm for Nd; 0.05 ppm for Sm, Gd, Dy, and Yb; 0.01 ppm for Tb, Tm, and Lu and 0.03 ppm for Er.

3. Results

3.1 Lithostratigraphy

3.1.1 Cerro Figurita Formation

The sedimentary sequence described as the CFFm crops out over an area of 100 km^2 close to the Sarandí del Yí Shear Zone in the Piedra Alta Terrane (Fig. 1). Northwards, the CFFm is in tectonic contact with Rhyacian granodiorites whereas in the southern area it is overlain by Cretaceous basalts (Fig. 3 and 4). The presence of a recrystallized illite and chlorite matrix in siliciclastic rocks of the CFFm indicates low-grade conditions during the metamorphism. The sequence is gently folded into a syncline structure. The fining-upward sequence is composed of four sedimentary facies, which from base to top are:

1) Fining upwards cycles of coarse polymictic conglomerates and subordinate intercalated lithic- and feldspathic arenites (750 meters thick).

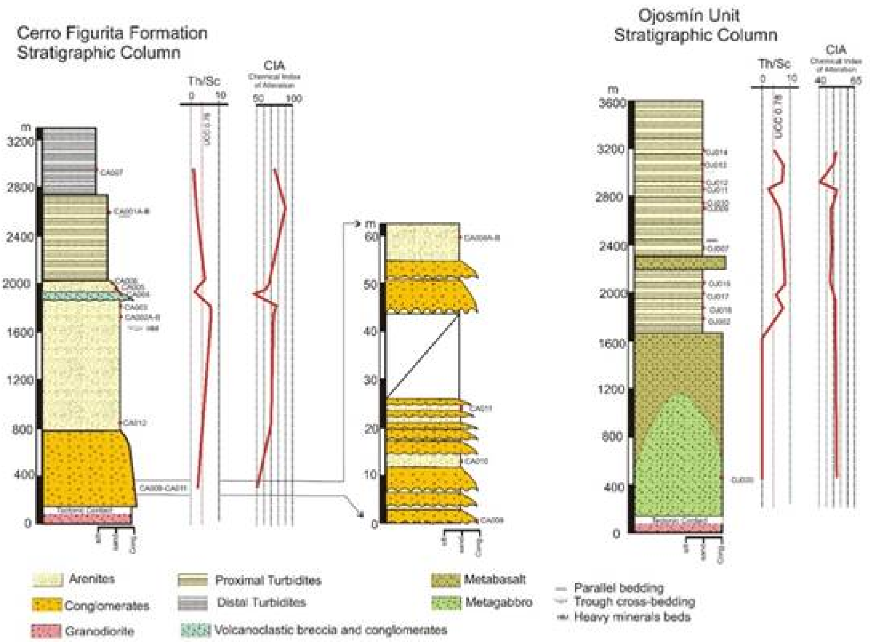

FIGURE 3
Stratigraphic columns of the CFFm and the OU. Note the Th/Sc and CIA variations along the stratigraphy give information about the weathering, source rocks and sediment recycling. See figures 4 and 5 for sample location

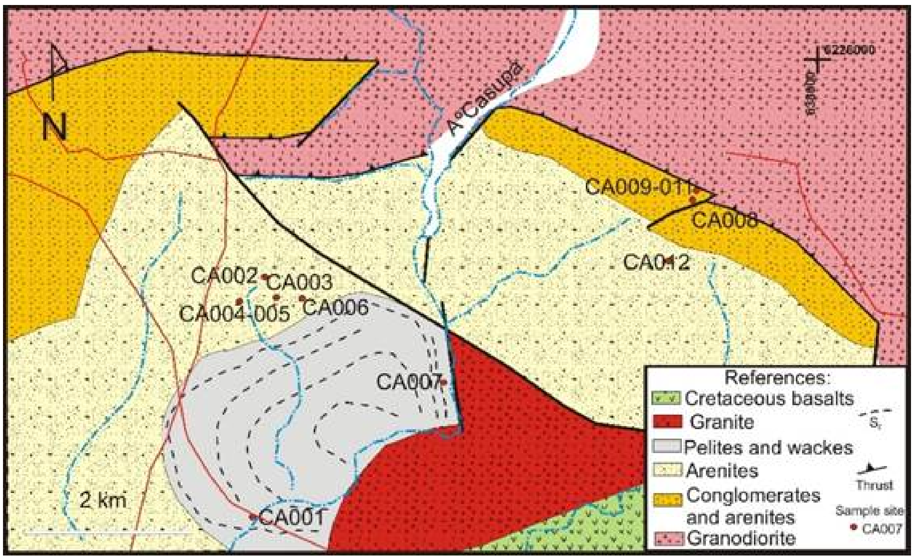

FIGURE 4
Geological map of the CFFm study area

2) The overlying unit is compositionally very immature and comprises acid and basic volcanic clasts and subordinate granitic and pelitic clasts (Fig. 5A-E). Erosive surfaces and gradational structures between

conglomerates and within conglomerates and arenites strata are reliable polarity indicators. Basement clasts are scarce. The thickness is 250 meters. Up section, arenites are more common. Stream deposits of unchannelized conglomerates represent alluvial fans.

3) Middle section, fine- to coarse-grained, feldspathic and quarzitic litharenites dominate and are up to 1200 meters in thickness. The arenites are poorly sorted, and the clayey matrix is due to alteration of labile lithoclasts. Polycrystalline quartz is common. Through cross-bedding and other sedimentary structures as well as thin layers of heavy mineral concentrates occur and suggest high energy of the fluvial system. Up section, volcanoclastic breccia and conglomerate, intercalated with wackes and litharenites, indicate a temporally and geographically closely related syn-sedimentary magmatism.

4) Up section two sedimentary facies are recognized: a) laminated green pelites, and b) wacke-pelite rhythmites, with a combined thickness of 500 meters. They are classified as proximal turbidites, probably related to a submarine fan.

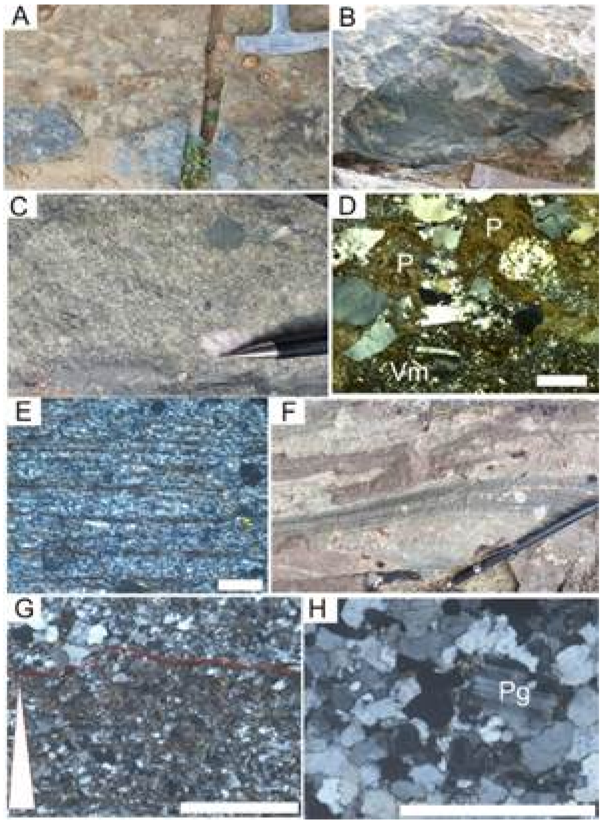

FIGURE 5

Outcrops and thin sections of the CFFm A coarse polymictic conglomerate B volcanoclastic breccia C conglomeratic sandstones D detrital pelite P and volcanic clasts Vm in a lithic arenite E alternation of detrital quartzfeldspar and illitechlorite laminae turbiditic facies OU F sandstone outcrop G normal grading in turbiditic sandstones H albitized plagioclase in fine sandstone showing concaveconvex grain contacts Scale bar represents 200 µm

5) At the top of the sequence, laminated grey pelites reach a thickness of 300 meters. The petrography reveals millimeter-thick interlayers of siltstones and claystones composed of reoriented clays dominated by illite and chlorite and angular clasts of quartz and feldspar (Fig. 5E). The accumulation of organic matter is another distinctive feature. The facies association suggests deep-water basin conditions during deposition of the top of the unit, and indicates a turbiditic environment.

CFFm represents a deepening-upward sequence (Fig. 3) indicating the evolution from an alluvial fan and braided fluvial-dominated environment to marine turbiditic conditions. The abundance of unstable lithoclasts, immaturity of the sandstones, and the thickness of conglomerate deposits point to a steep paleorelief linked to active tectonism during the sedimentation.

3.1.2 Ojosmín Unit

Bossi and Piñeyro[29] present the first comprehensive study of the Cerro Ojosmín area. The OU crops out over an area of 80 km^2 and comprises from base to top:

1) Serpentinized metagabbros and basic metavolcanic rocks, including high-magnesium ultrabasic rocks; tremolitic rocks, and MORB-derived metabasalts[28] (Fig. 6).

2) Metavolcano-sedimentary sequence composed of alternations of fine-grained metarenites (Fig. 5F), subordinate metapelites, and cherts, showing meter-thick tabular strata and scarce interlayers of basic metavolcanic rocks at the bottom. Feldspathic lithic arenite dominates the sequence in fining upward cycles (Fig. 5G-H). These sedimentary characteristics suggest turbiditic processes for the unit.

Some plagioclase grains show evidence of recrystallization and well-preserved albite-law twinning (Fig. 5H). Subordinate microcline feldspar shows grid twinning in cross-polarized light. Metamorphic minerals are common, such as biotite nests, euhedral sphene, and amphibole crystals, indicative of low to medium metamorphic grade.

3) Acid magmatism post-dates and intrudes the previous rocks, comprising sub-vertical dikes of microgranite and trachyte, and granophyres cropping out at the topographic high in the Cerros de Ojosmín.

In the northern area, the OU is overthrust by the Paleoproterozoic Cardona granodiorite. In the southern sector, pegmatites intruded along the thrust plane. Mainly based on geological considerations, Bossi and co-workers indicate that the granodiorite thrust occurred at 1900 ± 50 Ma, and the crystallization age of the porphyritic rocks is probably correlated to the acidic magmatism of the San José Belt at 1730 ± 10 Ma[29].

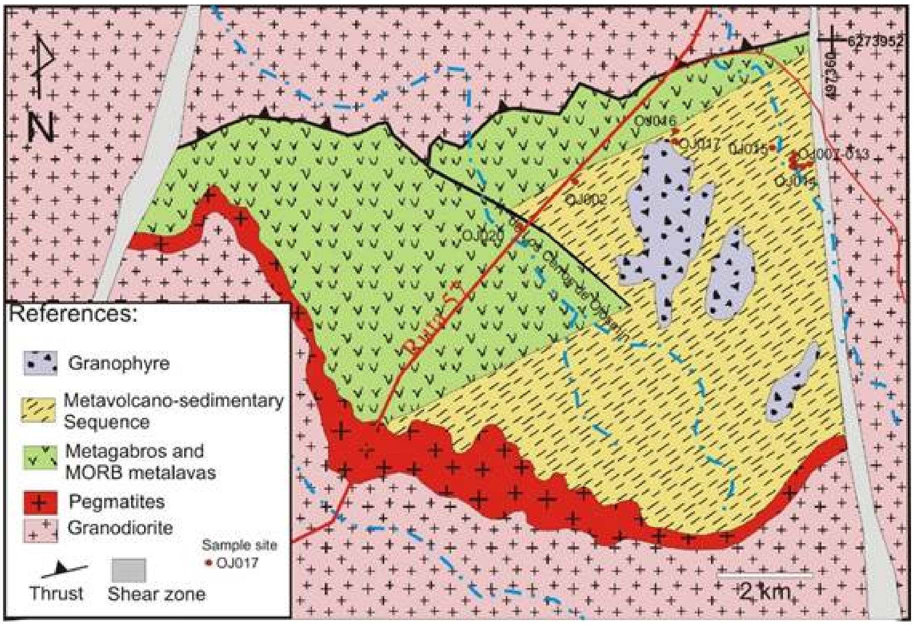

FIGURE 6
Geological map of OU study area
Modified after Bossi and Piñeyro[29]

3.2 Geochemistry

3.2.1 Major elements

The CFFm sedimentary rocks are characterized by low to high SiO_2/Al_2O_3 and K_2O/Na_2O ratios, whereas the Ojosmín turbidites show narrower ranges of variation (Fig. 7 and Table 1 of the supplementary material). The Ojosmín sample set shows Na_2O concentrations varying from 3.5 to 5.5%, indicating Na-plagioclase detrital contribution and/or Na redistribution during diagenesis or metamorphism. A few arenites of the CFFm display Na_2O values as high as 3.2%. Both units show low CaO concentrations (<2%), with few exceptions. The arenites interlayered with the conglomerates of the CFFm have CaO concentrations between 2 and 3.5%. Al_2O_3 concentration ranges from 12 to 18% and is related to the feldspar and clay content of the pelites and turbidites of the CFFm. Al_2O_3 abundances are between 11 to 12% for the metasedimentary rocks of the OU and indicate low maturity.

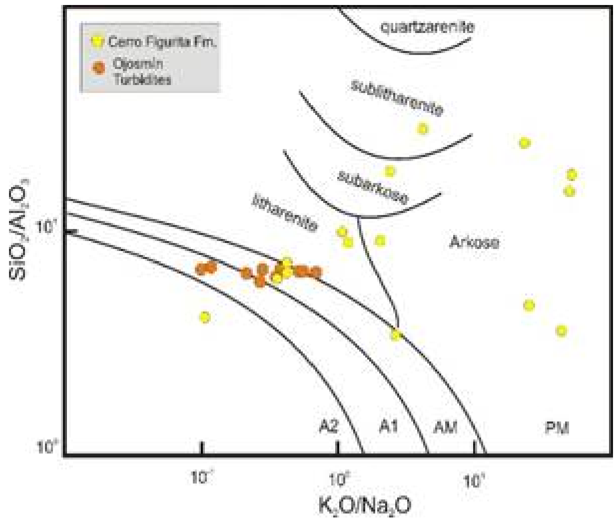

FIGURE 7

K_2O/Na_2O-SiO_2/Al_2O_3 after Roser and Korsh[31] and Pettijohn and Potter[32].
PM: passive Margin, AM: active margin, A1: arc setting, A2: evolved arc setting

3.2.2 REE and other trace elements (Tables 2 and 3 of the supplementary material)

High field strength elements, Th, Zr, Hf, Nb, and rare earth elements (REE) are insoluble and usually immobile under surface conditions preserving the source rock characteristics in the sedimentary record[19][33][34][35][36].

The diagram after Winchester and Floyd[37] is broadly used in sedimentary geochemistry to discriminate sedimentary source rock composition. Samples of the OU point to acid components (rhyolite field) whereas an intermediate to mafic composition (andesite and andesite/basalt fields) is related to the CFFm (Fig. 8), except for the quartzarenites occurring in the middle of the stratigraphic column (Fig. 3).

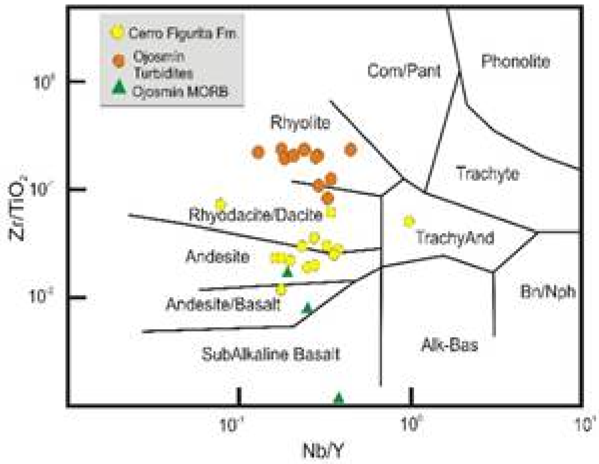

FIGURE 8
Nb/Y-Zr/TiO_2 diagram after Winchester and Floyd[37]

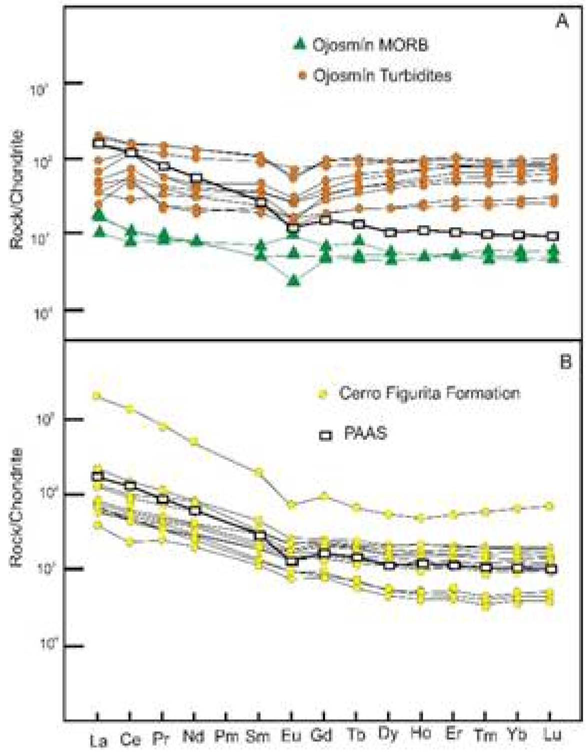

FIGURE 9
REE pattern for the studied units compared with Post Archean Australian Shales (PAAS)[38].
Note the relative depletion on LREE and the enrichment in HREE due to fractionation in OU when is compared with the PAAS. The CFFm shows a similar pattern compared to the PAAS

Chondrite-normalized REE patterns (Fig. 9 and Table 3) of the CFFm are parallel to the PAAS (Post Archaean Australian Shales)[38]. The metasedimentary rocks of the OU display a slight depletion in LREE and enrichment in HREE compared to PAAS, showing a flat REE pattern. La_N/Yb_N ratios <2 on average are far below the UCC average of 9.3[39].

Eu/Eu* values between 0.5 and 0.7 are typical for the UCC[39]; metasedimentary rocks of the OU show Eu/Eu* negative anomalies in the range of the UCC, spreading between 0.5 and 0.7, whereas for the CFFm the Eu/Eu* values are between 0.7 and 0.8, and indicate the Ca-plagioclase addition.

4. Discussion

Geochemical data presented here for the (meta)sedimentary rocks give relevant information to understand processes such as weathering, sorting, diagenesis, and metamorphism and give insights regarding the paleoclimate and tectonism[14][36][40][41][42][43][44] during deposition of both units.

4.1 Weathering and Post-Sediementary Alteration

4.1.1 Major and trace elements

Chemical weathering exerts a major control in the composition of siliciclastic detritus and is controlled by paleoclimatic and paleoweathering conditions[41]. To assess weathering the CIA (Chemical Index of Alteration)[18], PIA (Plagioclase Index of Alteration)[43], and Th/U vs Th tests were conducted[36].

Mobilization of major elements as a result of weathering is assessed using the CIA[18] in conjunction with A-CN-K ternary diagram[18][41] and in a similar way the PIA used the (A-K)-C-N diagram[43]. These indexes use molar proportions as follows: 1) CIA = (Al_2O_3 / (Al_2O_3 + CaO* + Na_2O + K_2O)) x 100, and 2) PIA = (Al_2O_3- K_2O) / (Al_2O_3 - K_2O) + CaO* + Na_2O).

Effectively, the CIA index mostly measures the degree of alteration of feldspars (since this group of minerals composes approximately 70% of the upper crust) and volcanic glass to clay minerals during weathering. The PIA index focuses on the alteration of plagioclase. The Th/U ratio of UCC is 3.8, and for most sedimentary rocks derived from the average upper crust the Th/U ratio is 3.5-4.0[33]. As detritus is subjected to weathering and/or recycling under oxidizing conditions, the Th/U ratio typically increases, because U^{4+} is oxidized to the more soluble U^{6+} species, and the latter is removed from sediments[36].

Ojosmín Unit.- Low CIA and Th/U values, 48 to 53 and 2.5 to 4.0, respectively, indicate almost no chemical weathering for the arenites of OU (Figs. 3 and 10A-C). The plagioclase abundance of the arenites appears related to the rapid unroofing of a plagioclase-rich source and to low intensity of chemical weathering. Post sedimentary Na-metasomatism probably affected OU to a low degree. Albitized plagioclase is detected in the OU arenites (Fig. 5H) and sodium metasomatism probably deviates some samples from a normal trend in the A-CN-K diagram toward the plagioclase apex (Fig. 10A). Low PIA values and oligoclase composition for the plagioclase suggested in the AK-C-N diagram (Fig. 10B) support a provenance from a non-altered granodioritic basement as a primary source rock component.

Such low CIA, PIA, and Th/U values for the OU probably indicate cold and arid climatic conditions during deposition[41][43][44]. These climatic conditions match the worldwide Rhyacian glaciations (Huronian), the GOE (Great Oxygenation Event), and the Lomagundi carbon isotope excursion documented at the top of the Paso Severino Formation[45] and in Tandilia[46].

4.1.2 REE

The REE patterns can be affected by: I the sorting of accessory minerals enriched in REEs, II mixing of upper crustal sources, or III fractionation during weathering, diagenesis or metamorphism[39].

The flat REE patterns observed for the OU sample set deviate from the PAAS, and rather than pointing to a mafic component of the source rocks indicate fractionation of the REE. The exceptionally high concentrations of Zr (295 to 560 ppm, average UCC=190 ppm), Hf, and Y are linked to the addition of the heavy mineral zircon. HREE like Erbium and Ytterbium are distinctly enriched, as shown by a deviation from UCC and a vertical trend (Fig. 12). In highly oxidizing conditions Ce^{3+} oxidizes to Ce^{4+} and is less readily removed from the system. Positive Ce/Ce* anomalies, observed in five samples with values from 1.6 to 2.3, suggest REE removal in an oxidizing environment and implies fractionation during diagenesis or metamorphism[42]. REE patterns parallel to the PAAS indicate no remobilization during diagenesis or metamorphism for the CFFm, although K-metasomatism is detected in some samples (Fig. 10).

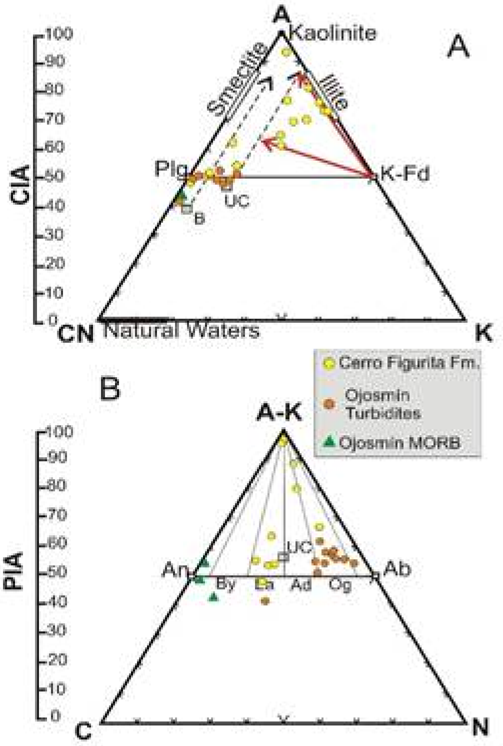

FIGURE 10

Chemical alteration of the analyzed rocks. A) Ternary A-CN-K (Al_2O_3-[CaO*+Na_2O]-K_2O) diagram; arrow-headed lines indicate normally predicted weathering trend[41] of average post-Archaean Upper Continental Crust (empty square denotes UCC and B unaltered basalt). The spread of the data indicate composition range from granodiorite to basalt. B) Ternary AK-C-N (Al_2O_3+K_2O)-CaO*-Na_2O. CIA: Chemical Index of Alteration. Note that most samples of Ojosmín turbidites plot in the bulk oligoclase field. PIA: Plagioclase Index of Alteration. An=anorthite, By=bytowinite, La=labradorite, Ad=andesine, Og=oligoclase, Ab=albite

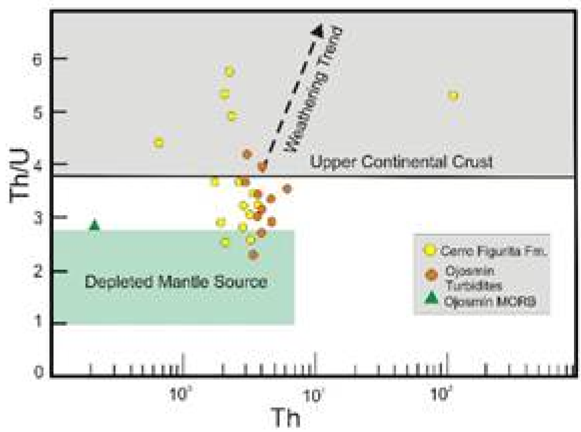

FIGURE 11
Th/U vs. U after McLennan and others[36]; see text for detailed discussion

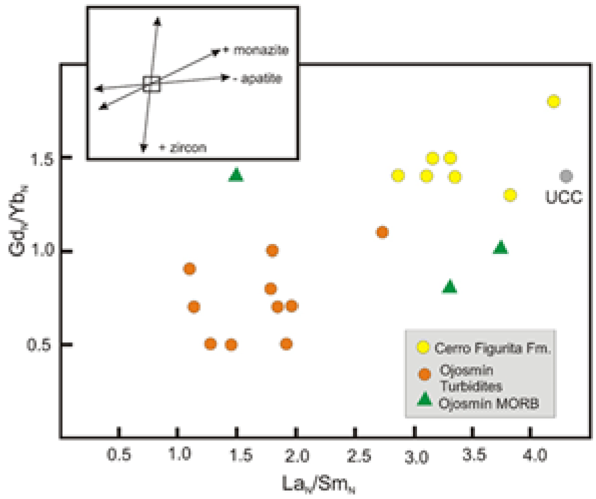

FIGURE 12
Gd_N/Yb_N vs. La_N/Sm_N after Bock and others[47] shows a vertical trend in the OU sample set, which is related to the effect of zircon addition

4.2 Age of Cerro Figurita Formation

The Piedra Alta Terrane rocks (including amphibolites, calc-alkaline granites, and the Paso Severino Formation) show a range of crustal residence between 2.1 to 2.4 Ga and $\varepsilon_{Nd(t)}$ values between -0.4 and 3.1. Metapelites of the Paso Severino Formation show T_{DM} model ages of 2.2 Ga[28] and $\varepsilon_{Nd(t)}$ between 2.1 and 2.5 and a precise sedimentation age of 2146 Ma[27]. The CFFm shows positive $\varepsilon_{Nd(t)}$ up to 3.5 and T_{DM} ages between 2.0 to 2.3 Ga, suggesting a maximum sedimentation age of *ca.* 2.0 Ga, at least 150 million years younger than the Paso Severino Formation. Therefore, positive $\varepsilon_{Nd(t)}$ and the low Th/Sc values around 0.1 (see Table 4 of the supplementary material) of most of the non-recycled samples of the CFFm indicate a juvenile crustal source component or at least low crustal contamination during deposition[30]. In any case, more precise geochronological evidence will help to better constrain the sedimentation age of the CFFm.

4.3 Provenance and Tectonic Setting

Ratios of certain immobile elements (e.g. Th/Sc, Zr/Sc, Cr/V, Ti/Nb, La/Sc) are robust provenance indicators when compared to average upper continental crust composition, revealing the compositional heterogeneity of the source rocks (Fig. 13)[14][21][39]. Ratios between an incompatible (Th) and a compatible element (Sc) reflect either the mafic or felsic composition of the source bulk, whereas the Zr elemental concentration indicates the recycling that resulted in the addition of the heavy mineral zircon. The geochemical source components are evaluated together with the geological and sedimentological features of the Paleoproterozoic units.

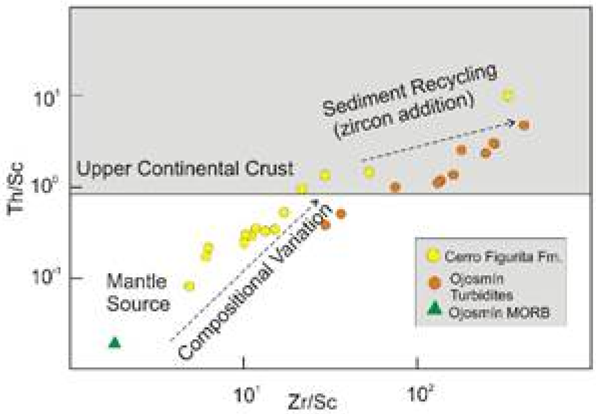

FIGURE 13
Th/Sc vs. Zr/Sc diagram[39]. Discussion in the text

A mantle source component for the CFFm is confirmed by low Th/Sc and Zr/Sc ratios compared to UCC composition and indicates scarce recycling. Moreover, high Cr/V (7-12) and low Y/Ni (1.4-1.8) of some samples suggest that such mafic component has an ophiolitic signature[47][48] (Fig. 14). Ti/Nb ratios range from 400 to 1400 in the CFFm and match MORB basalt composition, supporting a mafic source component in the provenance. The presence of volcanoclastic conglomerates and breccias reported in this work (Fig. 5. A-D) confirm the influence of a synsedimentary mafic source component probably during the Orosirian, as discussed above. A probable link between the MORB-like lavas of OU and the ophiolitic component of the CFFm provenance is suggested in this work, although a precise mineralogical analysis is needed to further support this.

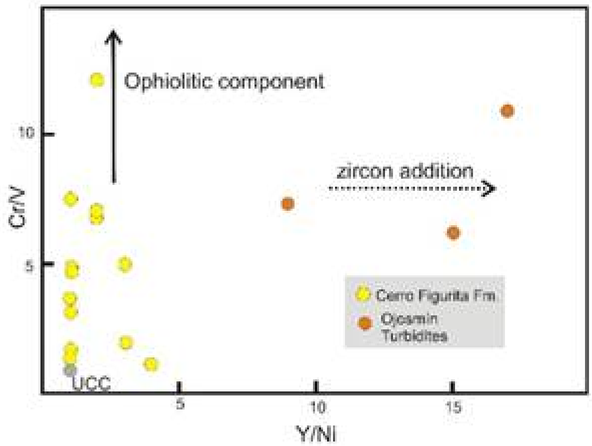

FIGURE 14
Cr/V vs. Y/Ni diagram Hiscott[48] shows the ophiolitic source rock component of CFFm and Y enrichment of Ojosmín turbidites due to zircon addition

Figure 13 shows derivation from felsic source rocks for the OU turbidites and recycling that resulted in the enrichment of the heavy mineral zircon during deposition. High Cr/V values ranging from 6 to 20 point to the presence of chromite (Cr between 130 and 294 ppm), probably added during recycling of a sedimentary source rock. Probable source rocks of the OU turbidites should account for the geochemical signature here deduced involving both mafic/ultramafic (old recycled) and felsic components. The juvenile felsic magmatism described in the Florida Arc could account for the granodioritic characteristics of the source component, whereas the mafic/ultramafic sources remain unidentified.

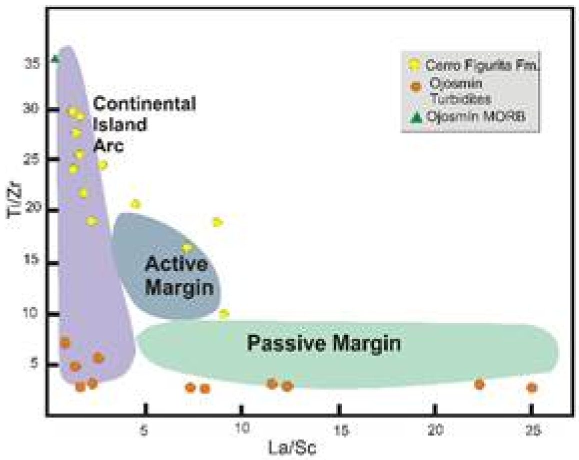

FIGURE 15
La/Sc vs. Ti/Zr discriminant diagram plot tectonic setting, after Bhatia and Crook[34]

Geochemical proxies such as low Ti/Nb <180 (UCC=300), high Y/Ni (15-66), and Eu/Eu* negative anomaly support the preponderance of the felsic over the mafic provenance component. The granodioritic source explains the significant accumulation of detrital Na-plagioclase preserved in the OU turbidites, as reflected in the petrography and the high Na_2O/K_2O ratio between 1.5 and 10. Figures 13 and 14 could be used to decipher the sedimentological recycling and source rock compositions during the deposition of the OU and the CFFm. Recycling clastic sources in more than one cycle of sedimentation and/or a rich zircon source component could explain the high Zr/Sc values between 30 and 400 of the OU turbidites. The zircon enrichment and the consequent Zr, Y, and Hf additions account for a certain degree of spread observed in the provenance diagram of the Figure 16. Some clues regarding the tectonic setting of the OU basin are provided by geochemical data of the metavolcanic rocks linked to MORB activity[29]. Notwithstanding, the sample OJ020 is an ultramafic rock with 25% of MgO content but with an Eu/Eu* negative anomaly evidencing crustal contamination during crystallization. High Mg, Cr, Ni content, and low TiO_2 suggest differentiation processes during crystallization probably related to an early volcanic arc (e.g. boninites) which evolved from a suprasubduction zone or plume activity. Thus, an incipient, shallow volcanic arc that explains the mafic component of the source of OU turbidites could be a plausible hypothesis, but more evidence is needed to confirm this.

The diagrams of figures 15 and 16 indicate sediment supply derived from a continental island arc or andesitic arc for the CFFm involving an active tectonic setting during deposition.

A plausible tectonic scenario for the evolution of the Andresito and San José Belts involves the closure and deformation of their sedimentary basins before deposition of the CFFm in a foreland setting (Fig. 17). Subduction towards the south and generation of a magmatic calc-alkaline arc, namely Florida, is a well-documented event[4] that occurred around 2.1 to 2.0 Ga. The Paso Severino Formation, according to different authors, was probably deposited in a back-arc basin.

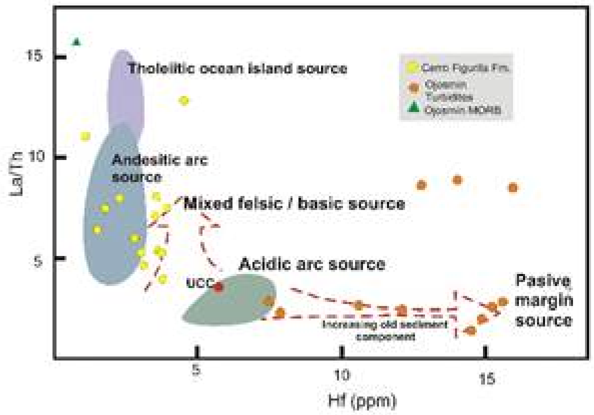

FIGURE 16

La/Th vs Hf discriminant diagram after Floyd and Levereridge[35] illustrating the radical change in provenance from a relatively unrecycled CFFm to an extremely reworked sediment for OU turbidites

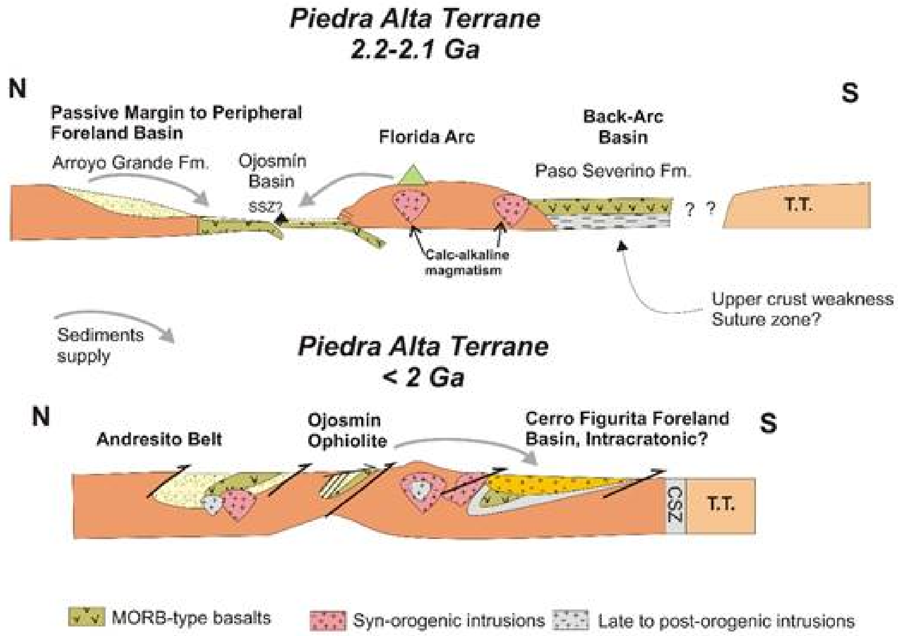

FIGURE 17
Sketch representing the paleogeographic evolution and the main source areas during the deposition of the OU and the CFFm during the Paleoproterozoic.
T.T.: Tandilia Terrane, SSZ: Suprasubduction Zone, CSZ: Colonia Shear Zone

After the final closure of the Paso Severino basin at ca. 2.08 Ga[26] uplift of the OU occurs and the calc-alkaline granodiorites (e.g. Cardona Granodiorite) are thrusted over the OU in the Piedra Alta Terrane. In this scenario, the OU would act as a probable source for CFFm. Synsedimentary magmatism coeval to deposition of the CFFm was related to the post-tectonic tectonothermal regime detected elsewhere in the Piedra Alta Terrane[7]. Facies analysis and geochemical proxies indicate evolution from non-recycled clastic continental to deep-marine turbiditic conditions. Sedimentation of the CFFm related to an active margin (Figs. 15 and 16) probably took place in a foreland geotectonic setting. Based on petrographic and geochemical proxies the source rock components are:

1. calc-alkaline granodiorites and acid to basic volcanic rocks.
2. Paso Severino Fm: meta volcano-sedimentary rocks, mostly meta-pelites and meta-basalts.

Ojosmín Ophiolites: mainly metabasalts with MORB affinities. Metaperidotites to metafelsic rocks. Clastic rocks are dominated by fine meta-arenites and meta-siltstones. However, it is fair to mention that confirmation of this source will provide a more robust tectonic model.

Minimum depositional age for the CFFm is indicated by the Florida Dike Swarm that intruded the Piedra Alta Terrane between 1.73 and 1.79 Ga[46]. The CFFm remained unaffected by the widespread extensional magmatism, although it was affected and bent by a Mesoproterozoic tectonothermal accretional event along the Sarandí del Yí Shear Zone[49][50]. In this work, a probably syn-sedimentary 1.9-2.0 magmatic event is suggested during the CFFm sedimentation based on Nd-isotopes[30] and provides a probable maximum depositional age for the sedimentary sequence. Nevertheless, more geochronological evidence is needed to confirm the 1.9-2.0 event in the Piedra Alta-Tandilia Terranes and the depositional age of the CFFm. Evidence of a complex tectono-magmatic scenario for the evolution of the RPC emerge in a diverse Paleoproterozoic sedimentary record. Interestingly, detrital zircon dating presented by Blanco and others[12] and Gaucher and others[51], reveals a major 1.9 Ga felsic magmatic event that sourced the Ediacaran Arroyo del Soldado Basin in the Piedra Alta and Nico Pérez Terranes which are part of the Río de la Plata Craton[12] [51].

5. Conclusions

Geochemistry of the OU turbidites and the CFFm give information about two poorly known, key Paleoproterozoic volcano-sedimentary sequences of the Piedra Alta Terrane.

The source area of OU turbidites underwent little weathering, probably related to the prevalent climate conditions during the worldwide Paleoproterozoic glaciations. Provenance based on geochemistry and sedimentological considerations indicates a source area composed of a recycled mafic/ultramafic component and a felsic non-recycled granodioritic unit.

Detritus was probably shed from the Florida Arc granodiorites and an incipient volcanic arc (in a supra subduction setting?), as revealed by geochemical data of mafic/ultramafic gabbros and MORB-like lavas.

The Cerro Figurita Formation is recognized as a new lithostratigraphic unit based on facies analysis, petrographic, geochemical, and geochronological data. The CFFm represents a deepening upward sequence, ranging from continental deposits in an alluvial fan-dominated environment at the base, to marine turbiditic conditions up section. The geochemistry indicates a provenance dominated by felsic and mafic source rock components and the detrital supply was probably derived from the Florida Arc, the Ojosmín Unit, and the Paso Severino Formation. The ongoing geochronological studies on the Paleoproterozoic meta-volcano-sedimentary units will shed light on the understanding of the geotectonic and crustal evolution of the Piedra Alta Terrane and the Río de la Plata Craton, testing the ideas here presented.

Acknowledgments

This work is dedicated to the memory of Professor Jorge Bossi, whom we consider the "father" of modern Uruguayan geology. Johana Castillo and Richards Villanueva assisted during the laboratory tasks performed at CURE. The Academic Cooperation Agreement between the PDU Geology and Mineral Resources from the Department of Geosciences of CURE (UdelaR) and the University of La Plata, Argentina (Museo de La Plata), helped to carry out fieldworks. We thank Thomas Will and an anonymous reviewer for the constructive comments on the manuscript. Claudio Gaucher and Antonella Celio are thanked for the efficient editorial handling.

References

1. Cordani UG, Sato K, Teixeira W, Tassinari CCG, Basei MAS. Crustal evolution of the South American Platform. In: Cordani UG, Milani EJ, Thomaz-Filho A, Campos DA, editors. Tectonic evolution of South America: 31th International Geological Congress, Rio de Janeiro, Brazil, August 6 - 17, 2000. Rio de Janeiro (BR): [publisher unknown]; 2000. p. 19-40.
2. Cingolani CA, Dalla Salda L. Buenos Aires cratonic region. In: Cordani UG, Milani EJ, Thomaz-Filho A, Campos DA, editors. Tectonic evolution of South America: 31th International Geological Congress, Rio de Janeiro, Brazil, August 6 - 17, 2000. Rio de Janeiro (BR): [publisher unknown]; 2000. p. 139-46.
3. Bossi J, Cingolani C. Extension and General Evolution of the Río de la Plata Craton. Developments in Precambrian Geology. 2009;16:73-85.
4. Sánchez Bettucci L, Peel E, Oyhantçabal P. Precambrian geotectonic units of the Río de la Plata craton. Int Geol Rev. 2010;52(1):32-50.

5. Santos JOS, Chernicoff CJ, Zappettini EO, McNaughton NJ, Greau Y. U-Pb geochronology of Martín García, Sola, and Dos Hermanas Islands (Argentina and Uruguay): Unveiling Rhyacian, Statherian, Ectasian, and Stenian of a forgotten area of the Río de la Plata Craton. J South Am Earth Sci [Internet]. 2017 [cited 2021 Aug 02];80:207-28. Available from: https://bit.ly/3rNGVDA.

6. Oyhantçabal P, Siegesmund S, Wemmer K. The Río de la Plata Craton: a review of units, boundaries, ages and isotopic signature. Int J Earth Sci. 2011;100(2):201-20.

7. Oyhantçabal P, Cingolani CA, Wemmer K, Siegesmund S. The Río de la Plata Craton of Argentina and Uruguay. In: Siegesmund S, Basei MAS, Oyhantçabal P, Oriolo S, editors. Geology of Southwest Gondwana. Cham (CH): Springer; 2018 [cited 2021 Aug 02]. p. 89-105. Available from: https://bit.ly/3jaD7IR.

8. Rapela CW, Fanning CM, Casquet C, Pankhurst RJ, Spalletti L, Poiré D, Baldo G. The Río de la Plata craton and the adjoining Pan-African/brasiliano terranes: their origins and incorporation into south-west Gondwana. Gondwana Res [Internet]. 2011 [cited 2021 Aug 02];20(4):673-90. Available from: https://bit.ly/3foVsRc.

9. Oriolo S, Oyhantçabal P, Konopásek J, Basei MAS, Frei R, Sláma J, Wemmerh K, Siegesmundh S. Late Paleoproterozoic and Mesoproterozoic magmatism of the Nico Pérez Terrane (Uruguay): tightening up correlations in southwestern Gondwana. Precambrian Res. 2019;327:296-313.

10. Abre P, Bossi J, Cingolani C, Gaucher C, Piñeyro D, Blanco G. El terreno Tandilia en Uruguay y Argentina. In: Bossi J, Gaucher C, editors. Geología del Uruguay. Vol. 1, Predevónico. Montevideo: PoloSA; 2014. p. 89-119.

11. Bossi J, Gaucher C. The Cuchilla Dionisio Terrane, Uruguay: an allochthonous block accreted in the Cambrian to SW-Gondwana. Gondwana Res. 2004;7(3):661-74.

12. Blanco G, Rajesh HM, Gaucher C, Germs GJB, Chemale F. Provenance of the Arroyo del Soldado Group (Ediacaran to Cambrian, Uruguay): Implications for the paleogeographic evolution of southwestern Gondwana. Precambrian Res. 2009;171(1-4):57-73.

13. Blanco G, Germs GJB, Rajesh HM, Chemale F, Dussin IA, Justino D. Provenance and paleogeography of the Nama Group (Ediacaran to early Palaeozoic, Namibia): Petrography, geochemistry and U-Pb detrital zircon geochronology. Precambrian Res. 2011;187(1-2):15-32.

14. Abre P, Blanco G, Gaucher C, Frei D, Frei R. Provenance of the Late Ediacaran Rocha Formation, Cuchilla Dionisio Terrane, Uruguay: Tectonic implications on the assembly of Gondwana. Precambrian Res [Internet]. 2020 [cited 2021 Aug 02];342:105704. Available from: https://bit.ly/3xeoGbz.

15. Cingolani CA, Varela R. Examen geocronológico por el método Rubidio-Estroncio de las rocas ígneas de las Sierras Australes Bonaerenses. In: Actas del 5 Congreso Geológico Argentino. Buenos Aires: Librart; 1973. p. 349-71.

16. Rapela CW, Pankhurst RJ, Casquet C, Fanning CM, Baldo EG, González-Casado JM, Galindo C, Dahlquist JA. The Río de la Plata craton and the assembly of SW Gondwana. Earth-Science Rev. 2007;83(1-2):49-82.

17. Cingolani C. The Tandilia System of Argentina as a southern extension of the Río de La Plata craton: an overview. Int J Earth Sci. 2010;100:221-42.

18. Nesbitt HW, Young GM. Early proterozoic climates and plate motions inferred from major element chemistry of lutites. Nature. 1982;299:715-7.

19. Taylor SR, McLennan, SM. The Continental Crust: Its Composition and Evolution. Oxford: Blackwell; 1985. 312 p.

20. Bahlburg H, Vervoort JD, Du Frane SA, Bock B, Augustsson C, Reimann C. Timing of crust formation and recycling in accretionary orogens: insights learned from the western margin of South America. Earth-Science Rev [Internet]. 2009 [cited 2021 Aug 02];97(1-4):215-41. Avaiable from: https://bit.ly/3C6j72x.

21. McLennan SM, Taylor SR, Hemming SR. Composition, differentiation, and evolution of continental crust: constrains from sedimentary rocks and heat flow. In: Brown M, Rushmer T, editors. Evolution and differentiation of the continental crust. Cambridge: Cambridge University Press; 2006. p. 92-134.

22. Preciozzi F, Spoturno J, Heinzen W, Rossi P. Carta Geológica del Uruguay a escala 1/500.000. Montevideo: DINAMIGE; 1985. 90p.

23. Bossi J, Ferrando L. Carta geológica del Uruguay: a escala 1:500.000. Montevideo: Facultad de Agronomía; 2001. 1 CD-ROM.

24. Peel E, Preciozzi F. Geochronologic Synthesis of the Piedra Alta Terrane, Uruguay. In: Simposio Sudamericano de Geología Isotópica = South American Symposium on Isotope Geology. Montevideo: SSAGI; 2006. p. 234-7.

25. Ribot AM, Bossi J, Cingolani CA, Piñeyro D. Caracterización petrográfica y cinemática de la faja milonítica Colonia - Arroyo Pavón en el sur del Terreno Piedra Alta, Uruguay: zona de cizalla principal en basamento precámbrico? In: Actas XVI Congreso Geológico Argentino. Vol 1. La Plata (AR): Universidad de La Plata; 2005. p. 457-64.

26. Hartmann LA, Piñeyro D, Bossi J, Leite JAD, McNaughton NJ. Zircon U-Pb SHRIMP dating of Palaeoproterozoic Isla Mala granitic magmatism in the Río de la Plata Craton, Uruguay. J South Am Earth Sci. 2000;13:105-13.

27. Santos JOS, Hartmann LA, Bossi J, Campal N, Schipilov A, Piñeyro D, McNaughton NJ. Duration of the trans-amazonian cycle and its correlation within South America based on U-Pb shrimp geochronology of the la Plata craton, Uruguay. Int Geol Rev. 2003;45(1):27-48.

28. Pamoukaghlián K, Gaucher C, Frei R, Poiré DG, Chemale F, Frei D, Will TM. U-Pb age constraints for the La Tuna Granite and Montevideo Formation (Paleoproterozoic, Uruguay): unravelling the structure of the Río de la Plata Craton. J South Am Earth Sci. 2017;79:443-58.

29. Bossi J, Piñeyro D. Terreno Piedra Alta. In: Bossi J, Gaucher C, editors. Geología del Uruguay. Vol 1, Predevónico. Montevideo: Polo; 2014. p. 45-86.

30. Blanco G, Abre P, Frei D, Cingolani C, Lanfranchini M, Ferrizo H, Uriz N. Petrografía, Geoquímica y Sm/Nd como indicadores de proveniencia en la formación Paso Severino, Cratón del Rio de la Plata, Uruguay. In: IX Congreso Uruguayo de Geología, V Simposio LAC sobre geoparques; 2019 November 4-8; Trinidad, Uruguay: resúmenes [Internet]. 2019 [cited 2021 Aug 02]. p. 55. Available from: https://bit.ly/3rLLzCh.

31. Roser BP, Korsch RJ. Determination of tectonic setting of sandstone-mudstone suites using SiO_2 content and K_2O/Na_2O-ratio. J Geol. 1986;94(5):635-50.

32. Pettijohn FJ, Potter, PE, Siever R. Sand and Sandstones. New York: Springer; 1972. 618p.

33. McLennan SM, Taylor SR, McCulloch MT, Maynard JB. Geochemical and Nd-Sr isotopic composition of deep-sea turbidites: crustal evolution and plate tectonic associations. Geochim Cosmochim Acta. 1990;54:2015-50.

34. Bhatia MR, Crook KAW. Trace element characteristics of graywackes and tectonic setting discrimination of sedimentary basins. Contrib to Mineral Petrol. 1986;92(2):181-93.

35. Floyd PA, Leveridge BE. Tectonic environment of the Devonian Gramscatho basin, south Cornwall: framework mode and geochemical evidence from turbidite sandstones. J Geol Soc London. 1987;144:531-42.

36. McLennan SM, Hemming S, McDaniel DK, Hanson GN. Geochemical approaches to sedimentation, provenance and tectonics: processes controlling the composition of clastic sediments. Spec Pap Geol Soc Am. 1993;284:21-40.

37. Winchester JA, Floyd PA. Geochemical discrimination of different magma series and their differentiation products using immobile elements. Chem Geol. 1977;20:325-43.

38. Nance WB, Taylor SR. Rare earth element patterns and crustal evolution: I. Australian post-Archean sedimentary rocks. Geochim Cosmochim Acta. 1976;40:1539-51.

39. McLennan SM, Bock B, Hemming SR, Horrowitz JA, Lev SM, McDaniel DK, The roles of provenance and sedimentary processes in the geochemistry of sedimentary rocks. In: Lentz RD, editor. Geochemistry of sediments and sedimentary rocks: evolutionary considerations to mineral-deposit-forming environments. St. John's (CA): Geological Association of Canada; 2003. p. 7-38.

40. Blanco G, Abre P, Ferrizo H, Gaye M, Gamazo P, Ramos J, Alvareda E, Saracho A. Revealing weathering, diagenetic and provenance evolution using petrography and geochemistry: a case of study from the Cretaceous to Cenozoic sedimentary record of the SE Chaco-Paraná basin in Uruguay. J South Am Earth Sci [Internet]. 2021 [cited 2021 Aug 02];105:102974. Available from: https://bit.ly/2V63Cr3.

41. Nesbitt HW, Young GM. Prediction of some weathering trends of plutonic and volcanic rocks based on thermodynamic and kinetic considerations. Geochim Cosmochim Acta. 1984;48:1523-34.

42. Fedo CM, Wayne, Nesbitt H, Young GM. Unraveling the effects of potassium metasomatism in sedimentary rocks and paleosols, with implications for paleoweathering conditions and provenance. Geology. 1995;23:921-4.

43. Fedo CM, Young GM, Nesbitt HW, Hanchar JM. Potassic and sodic metasomatism in the Southern Province of the Canadian Shield: evidence form the Paleoproterozoic Serpent Formation Huronian Supergroup, Canada. Prec Res. 1997;84:17-36.

44. Nesbitt HW. Petrogenesis of siliciclastic sediments and sedimentary rocks. In: Lentz RD, editor. Geochemistry of sediments and sedimentary rocks: evolutionary considerations to mineral-deposit-forming environments. St. John's (CA): Geological Association of Canada; 2003. p. 39-51.

45. Maheshwari A, Sial AN, Gaucher C, Bossi J, Bekker A, Ferreira VP, Romano AW. Global nature of the Paleoproterozoic Lomagundi carbon isotope excursion: a review of occurrences in Brazil, India, and Uruguay. Precambrian Res. 2010;182:274-99.

46. Lajoine MF, Sial A, Ballivian CA, Cingolani CA, Recio C, Etcheverry RO, Basei MAS, Lanfranchini ME. First geochronological constraint for the Palaeoproterozoic Lomagundi-Jatuli δ13C anomaly in the Tandilia Belt basement (Argentina), Río de la Plata Craton. Prec Research [Internet]. 2019 [cited 2021 Aug 02];334:105477. Available from: https://bit.ly/2VlejWi.

47. Bock B, McLennan SM, Hanson GN. Geochemistry and provenance of the Middle Ordovician Austin Glen Member (Normanskill Formation) and the Taconian Orogeny in New England. Sedimentology. 1998;45:635-55.

48. Hiscott RN. Ophiolithic source rocks for Taconic-age flysh: trace element evidence. Geol Soc Am Bull. 1984,95:1261-7.

49. Bossi J, Campal N. Magmatismo y tectónica transcurrente durante el Paleozoico inferior del Uruguay. In: Gutiérrez J, Saavedra J, Rábano I, editors. Paleozoico Inferior de Ibero-América: Alicante: Universidad de Extremadura; 1992. p. 343-56.

50. Gaucher C, Frei R, Samaniego L, Will TM, Chemale F, Gargiulo MF, Poiré DG, Ling X, Li XH, Li QL. The Tapes Complex (Nico Pérez Terrane, Uruguay): Constraining the Mesoproterozoic evolution of the Río de la Plata Craton. J South Am Earth Sci [Internet]. 2021 [cited 2021 Aug 02];105:102906. Available from: https://bit.ly/3ihyMEs.

51. Gaucher C, Finney S, Poiré D, Valencia V, Grove M, Blanco G, Paoumukaghlian L, Peral L. Detrital zircon ages of Neoproterozoic sedimentary successions in Uruguay and Argentina: insights into the geological evolution of the Río de la Plata Craton. Prec Research. 2008;167:150-70.

Supplementary material

TABLE 1
Major element data of the OU and CFFm expressed in %. L/F: Lithology/facies. Ar: arenites. T: turbidites, UB and G: metavolcanic rocks. Cg: conglomerates. VCg: volcaniclastic conglomerates. Pe: pelites. Va: wackestone

Unit	L/F	sample	SiO_2	Al_2O_3	Fe_2O_3	MgO	CaO	Na_2O	K_2O	TiO_2	MnO	LOI	Sum	CIA
Ojosmin	Ar-T	OJ002	76,17	1152	3,85	0,02	0,41	5,46	1,18	0,2		1,0	99,92	51
	Ar-T	OJ016	75,64	11,15	4,9	0,07	0,69	4,83	1,4	0,23	0,01	0,9	99,89	51
	Ar-T	OJ017	76,08	10,74	5,44	0,06	191	4,03	0,48	0,34	0,02	0,7	99,92	50
	Ar-T	OJ015	75,2	1125	4,04	0,06	1,14	4,6	2,38	0,23	0,07	0,7	99,84	48
	Ar-T	OJ007	75,44	1131	3,84	0,04	0,88	4,42	2,54	0,25	0,06	0,9	99,85	49
	Ar-T	OJ009	74,56	112	4,07	0,4	1,87	3,99	1,57	0,26	0,09	1,7	99,85	49
	Ar-T	OJ010	74,91	11,13	4,24	0,27	1,13	3,51	2,51	0,25	0,07	1,8	99,89	51
	Ar-T	OJ011	75,64	1174	3,49	0,22	1,26	4,05	1,48	0,23	0,04	1,7	99,92	53
	Ar-T	OJ012	72,53	10,46	5,32	1,17	5,34	3,39	0,34	0,22	0,12	0,9	99,83	40
	Ar-T	OJ013	75,88	11	3,93	0,32	0,98	4,54	1,79	0,23	0,07	1,0	99,82	50
	Ar-T	OJ014	73,05	12,12	4,77	0,56	1,6	4,59	1,24	0,36	0,06	1,4	99,92	51
	UB	OJ020	49,12	6,42	8,46	24,78	3,07	0,04	0,02	0,16	0,15	6,9	99,56	53
	UB	UB	45,1	8,7	9,7	23,8	5,2	0,2	0,1	0,2			6,2	47
	G	G	45,5	15,8	16,5	6,2	10,6	1,8	0,2	13			16	41
Cerro Figurita	Ar-Cg	CA010	78,44	7,88	3,67	0,75	3,05	138	1,52	0,34	0,06	2,7	99,93	45
Formation	Ar-Cg	CA011	77,9	8,6	4,91	1,02	2,06	132	1,6	0,45	0,05	1,8	99,91	53
	Ar-Cg	CA008A	74,62	10,31	4,84	1,28	3,14	2,25	0,96	0,52	0,06	1,7	99,9	50
	Ar-Cg	CA008B	73,06	10,73	5,32	1,47	3,54	2,24	0,96	0,56	0,06	1,8	99,88	49
	Ar	CA012	93,66	3,19	0,92	0,1	0,02	0,21	0,92	0,05	0	0,8	99,99	70
	Ar+HM	CA002A	48,23	3,14	36,67	0,09	0,01	0,02	1,05	7,92	0,29	1,1	98,96	73
	Ar	CA002B	90,43	4,98	137	0,13	0	0,03	1,68	0,17	0	0,0	99,97	73
	Ar	CA003	92,52	3,69	152	0,05	0,01	0,04	0,99	0,19	0	0,8	99,98	76
	VCg	CA004	57,14	13,73	11,68	3,5	5,52	3,15	0,33	1,21	0,15	3,2	99,82	47
	ArCg	CA005	80,96	8,84	3,66	0,52	0,43	107	2,23	0,44	0,02	1,6	99,94	64
	Ar	CA006	90,09	4,76	191	0,13	0,02	0,5	1,25	0,18	0,01	1,0	99,97	68
	Pe	CA007	62,09	17,54	7,06	2,34	0,37	104	2,82	0,7	0,04	5,7	99,86	76
	Pe-T	CA001A	67,44	18,31	2,05	0,7	0,26	0,08	3,71	0,64	0,02	6,5	99,89	80
	Pe-T	CA001B	74,22	15,71	137	0,15	0,26	0,03	0,8	0,63	0	6,4	99,88	92
	Va-T	CA001C	73,47	1186	4,92	1,61	0,75	2,86	1,05	0,54	0,04	2,6	99,9	62
		UCC	66	15,2	4,5	2,2	4,2	3,9	3,3805	0,64	0,077			46

TABLE 2

Trace element concentration of OU and CFFm samples, expressed in ppm

Unit	sample	Cr	Ba	Sc	Co	Cs	Ga	Hf	Nb	Rb	Sr	Ta	Th	U	V	W	Zr	Y	Mo	Cu	Pb	Zn	Ni	As
Ojosmin	OU002	178	430	1	2.8		23.6	12.1	22.9	10.6	48	1.3	4.9	1.7	9	1.3	410	84	10.2	3.8	1.2	8	5.0	0.6
	OU016	130	405	3	3		21.9	15.6	31.7	11.9	62	2.2	7.7	2.1	21	0.8	548	72	6.2	3.7	1.4	10	4.9	0.8
	OU017	164	373	5	2.8		18.8	10.6	19	5.8	138	1.2	4.9	1.2	14	1.3	374	66	9.3	3.2	1.4	16	2.8	
	OU015	260	676	2	0.8		21.7	16	25	41.1	55	1.8	5.9	1.9	20	1.4	560	141	16	2	2.1	12.7	2.2	
	OU007	212	849	2	0.7		22	14	24.2	37.4	57	1.5	5	1.5	14	2.1	508	131	14	2.7	3.4	178	2.0	0.6
	OU009	144	1122	4	1.2	0.2	22.1	14.9	21.1	37.8	88	1.3	4.7	1.3	13	1	544	10.3	8.7	3.4	1.7	243	2.1	1
	OU010	150	78.2	4	1.4	0.2	19.2	14.5	19.6	31.5	60	1.3	4.5	1.4	13	1	536	69	9	5.5	1.5	97	2.8	1.2
	OU011	144	407	8	1.3		15.5	7.5	12	22.3	70	0.9	3.9	0.9	13	1.6	29.5	35	9.5	8.8	1.4	131	2.1	1
	OU012	294	13.2	3	1		26.7	12.8	18.6	2.6	165	1.4	4.3	1.7	19	2	481	14.5	17.4	2.1	1.6	72	2.2	0.5
	OU013	150	507	2	0.9	0.2	22.4	15.3	25.4	28.2	43	1.7	5.9	1.7	21	1.1	548	10.7	11.2	9.8	6.4	10.2	1.8	0.5
	OU014	219	358	10	3.5	0.3	13.2	7.9	12	24.8	86	0.8	3.8	1	30	1.8	29.8	37	13	3.3	1.9	52	4.3	
	OU020	1813	8	15	84.2		5.2	0.8	1.4	0.3	5		0.3	0.1	60		2.8	7	0.6	1.1		30	478.7	
	UB	0	3.01	23					2	1	13						16	8						
	G	0	150	40					3	3	219						15	8						
Cerro Figurita	CA010	267	444	7	9.5	0.8	8.4	2.3	2.8	43.9	149	0.3	2.5	0.8	55	1.5	8.2	17	11.6	11.1	1.3	28	13.8	1.3
Formation	CA011	274	52.9	11	13.7	1.9	10.1	3	3.6	56.9	199	0.3	2.7	1	72	1.7	112	21	11.4	16.5	1.7	43	16.9	1.8
	CA008A	280	409	11	10.9	0.4	10.9	3.1	3.9	27.6	263	0.3	3.4	0.9	82	1.6	112	20	12.3	25.9	1.7	46	20.4	1.5
	CA008B	267	399	12	13.8	0.6	11.1	3.7	4.3	28.3	3.01	0.3	3.6	1.2	87	2.5	13.1	25	11	24.6	1.6	53	20.8	2.1
	CA012	404	427	0	2.6	1.9	2.3	1.1	0.5	21.1	16	0	0.9	0.2	33	2.7	3.8	6	20.4	3.5	1.8	3	3.6	0
	CA002A	2025	615	12	39.8	1.2	8.1	106.4	72.3	29.4	35	5.6	122.2	22.6	106.4	13.1	4087	75	8.8	4.8	40.4	11	27.2	2.9
	CA002B	335	757	2	3.4	1.1	4.3	2.8	2.3	41.5	15	0.2	3	0.6	49	2.2	104	7	15.5	4	2.3	3	3.7	0.6
	CA003	404	357	2	1.2	0.8	2.9	1.5	1.8	24.8	30	0.2	2.7	0.5	57	2.3	60	8	19.4	3.1	1.6	2	4.8	3.6
	CA004	246	224	30	35.7	0.2	14.7	3.6	5.3	11.1	291	0.4	2.3	0.6	153	0.7	148	31	7	29.1	1.9	94	32.3	2.7
	CA005	260	695	8	8	2.3	10.4	3.8	5.1	76	61	0.3	4.3	1.2	55	1.8	138	16	8.3	6.4	1.4	20	11.0	1
	CA006	445	311	3	3.9	1	3.8	1.8	2.2	32.5	25	0.2	2.9	0.5	59	2.5	6.6	8	20.6	3.5	1.9	5	5.9	0
	CA007	178	396	23	11.2	2.9	18.8	3.9	6.6	96.2	122	0.4	4.1	1.3	139	1.1	140	26	4.3	40.3	2.8	66	29.4	6.5
	CA001A	164	663	21	4.1	7.4	19.6	3.5	6.2	148.5	97	0.5	4.7	1.4	143	2	130	23	2.8	69.4	7	6	6.5	28.1
	CA001B	510	240	12	4.3	0.8	12.1	4.5	6.1	30.1	340	0.5	4.2	1.5	109	3.2	183	17	18	10.2	2	5	6.3	4.7
	CA001C	267	326	11	16.1	1.6	11.4	3.6	5.3	36.5	149	0.3	3.7	1.1	97	1.5	148	15	5.8	10.8	1.7	45	38.4	7.4
	UCC	83	550	13.6			17	5.8	12	112	350	1	10.7	2.8	97	1.9	190	22	1.1	25	17	71	44.0	4.8

TABLE 3
Rare Earth Element concentrations of OU and CFFm samples, expressed in ppm

Unit	sample	La	Ce	Pr	Nd	Sm	Eu	Gd	Tb	Dy	Ho	Er	Tm	Yb	Lu	ΣREE
Ojosmin	OJ002	11,6	28	4,15	17,8	5,77	0,79	7,42	1,66	12,79	3,28	10,97	1,78	12,18	1,97	120
	OJ016	22,3	83,5	5,36	19,7	5,16	0,8	6,91	1,57	11,31	2,83	9,2	1,52	10,55	1,8	183
	OJ017	12,8	48,1	4,07	18,2	5,65	1,55	7,48	1,53	10,51	2,54	8,15	1,25	8,32	1,33	131
	OJ015	49,9	108,5	14,26	60,8	16,29	3,25	19,85	3,65	23,79	5,38	16,85	2,48	15,95	2,52	343
	OJ007	44,6	97,7	13,59	60,7	15,78	3,17	19,5	3,55	22,68	4,96	14,27	2,12	13,87	2,15	319
	OJ009	9,2	18,3	3,25	15,1	5,27	1,52	8,52	2,02	15,64	4,02	12,89	1,99	13,29	2,12	113
	OJ010	6,2	34	2,18	9,4	3,44	1	5,82	1,4	10,63	2,67	9,01	1,39	9,88	1,66	99
	OJ011	11,4	34,8	4,11	15	3,91	0,89	4,05	0,83	5,54	1,31	3,92	0,62	4,2	0,67	91
	OJ012	37,1	82,3	11,12	48,2	13,04	4,14	16,82	3,26	22,63	5,47	16,78	2,4	14,78	2,22	280
	OJ013	16,2	73	4,83	21,6	7,12	1,75	10,56	2,39	17,2	4,08	12,97	2,01	13,14	2,11	189
	OJ014	8,8	37,5	2,4	10,4	2,85	0,74	3,97	0,82	5,75	1,44	4,75	0,73	4,86	0,74	86
	OJ020	4,7	7,1	0,92	3,7	0,79	0,14	1,08	0,18	1,13	0,28	0,88	0,12	0,88	0,13	22
	UB	4,2	6,8	0,94	3,7	0,8	0,33	1	0,2	1,3	0,3	0,9	0,16	1	0,16	22
	G	2,6	5,1	0,81	3,9	1,1	0,57	1,4	0,3	1,5	0,3	0,9	0,13	0,8	0,12	20
Cerro Figurita	CA010	19,9	32,7	4,12	15,5	3	0,75	3,06	0,47	2,88	0,61	1,9	0,25	1,65	0,25	87
Formation	CA011	14,2	31,8	3,56	14,9	3,11	0,82	3,41	0,58	3,56	0,79	2,42	0,32	2,13	0,35	82
	CA008A	15,9	38,2	3,81	15,2	3,23	0,9	3,38	0,53	3,29	0,69	2,2	0,3	2,09	0,29	90
	CA008B	19,2	40,1	4,61	18	3,66	1	4,1	0,67	4,1	0,92	2,64	0,4	2,57	0,37	102
	CA012	10	15,2	2,48	9,7	2,01	0,54	1,76	0,22	1,21	0,23	0,72	0,09	0,62	0,1	45
	CA002A	478,2	856,2	75,8	237,4	28,9	4,29	19,45	2,53	13,61	2,75	8,82	1,43	10,81	1,79	1742
	CA002B	18,1	30,3	3,63	14	2,45	0,53	1,89	0,25	1,42	0,27	0,7	0,11	0,72	0,11	74
	CA003	17,3	31	3,28	11,4	1,86	0,46	1,76	0,25	1,39	0,29	0,82	0,1	0,72	0,11	71
	CA004	18,6	36	4,46	18,8	4,54	1,25	5,13	0,85	5,13	1,19	3,43	0,49	3,2	0,47	104
	CA005	17,4	28,4	4,43	16,8	3,28	0,7	3,23	0,5	3,08	0,61	1,91	0,28	1,99	0,31	83
	CA006	21,7	38	4,17	15,5	2,29	0,56	1,99	0,27	1,44	0,28	0,89	0,11	0,81	0,12	88
	CA007	30,9	55,5	7,23	28,6	5,11	1,21	4,83	0,76	4,55	0,96	3,05	0,43	2,82	0,44	146
	CA001A	33,9	61,1	9,04	38,2	6,77	1,45	5,18	0,73	4,02	0,8	2,53	0,36	2,29	0,38	167
	CA001B	54,2	92,6	11,17	39,2	4,86	1,06	3,36	0,48	2,91	0,57	1,99	0,28	1,91	0,3	215
	CA001C	20	36,3	4,6	18,1	3,26	0,94	2,99	0,47	2,72	0,61	1,78	0,24	1,79	0,25	94
	UCC	38,2	80	8,9	32	5,6	1,1	4,7	0,77	4,4	1	2,9	0,4	2,8	0,43	183

TABLE 4
Selected element ratios of OU and CFFm samples

Unit	sample	Th/Sc	Th/U	Zr/Sc	Rb/Sr	La/Th	La/Sc	Cr/V	Cr/Th	Y/Ni	Ti/Nb	Ti/Zr	Eu/Eu*	Nb/Y	Sm/Nd	Rb/Sr	La/Nb	Lan/Ybn	Ce/Ce*	Gdn/Ybn
Ojosmin	OJ002	4,9	2,9	409,9	0,2	2,4	11,6	19,8	36	16,7	52,3	2,9	0,3	0,3	0,3	0,2	0,5	0,6	1,0	0,5
	OJ016	2,6	3,7	182,8	0,2	2,9	7,4	6,2	17	14,6	43,5	2,5	0,4	0,4	0,3	0,2	0,7	14	19	0,5
	OJ017	1,0	4,1	74,9	0,0	2,6	2,6	11,7	34	23,5	107,3	5,4	0,7	0,3	0,3	0,0	0,7	1,0	16	0,7
	OJ015	3,0	3,1	280,1	0,7	8,5	25,0	13,0	44	63,9	55,1	2,5	0,5	0,2	0,3	0,7	2,0	2,1	1,0	1,0
	OJ007	2,5	3,3	253,8	0,7	8,9	22,3	15,1	42	65,6	61,9	3,0	0,6	0,2	0,3	0,7	18	2,2	0,9	1,1
	OJ009	12	3,6	135,9	0,4	2,0	2,3	11,0	31	48,9	73,9	2,9	0,7	0,2	0,3	0,4	0,4	0,5	0,8	0,5
	OJ010	1,1	3,2	134,0	0,5	14	16	11,6	33	24,7	76,5	2,8	0,6	0,3	0,4	0,5	0,3	0,4	2,3	0,5
	OJ011	0,5	4,3	36,8	0,3	2,9	14	11,0	37	16,7	114,9	4,7	0,6	0,3	0,3	0,3	1,0	18	13	0,8
	OJ012	14	2,5	160,4	0,0	8,6	12,4	15,5	68	66,0	70,9	2,7	0,8	0,1	0,3	0,0	2,0	17	1,0	0,9
	OJ013	3,0	3,5	274,0	0,7	2,7	8,1	7,2	26	59,5	54,3	2,5	0,6	0,2	0,3	0,7	0,6	0,8	2,0	0,7
	OJ014	0,4	3,8	29,8	0,3	2,3	0,9	7,3	58	8,6	179,8	7,2	0,7	0,3	0,3	0,3	0,7	12	19	0,7
	OJ020	0,0	3,0	18	0,1	15,7	0,3	30,2	6042	0,02	685,0	34,9	0,5	0,2	0,2	0,1	3,4	3,6	0,8	1,0
	UB	0,0		0,7	0,1		0,2				599,4	74,9	1,1	0,3	0,2	0,1	2,1	2,8	0,8	0,8
	G	0,0		0,4	0,0		0,1				2597,4	519,5	13	0,4	0,3	0,0	0,9	2,2	0,8	14
Cerro Figurita	CA010	0,4	3,1	11,8	0,3	8,0	2,8	4,9	107	13	727,8	24,7	0,8	0,2	0,2	0,3	7,1	8,1	0,9	1,5
Formation	CA011	0,2	2,7	10,1	0,3	5,3	13	3,8	101	12	749,3	24,2	0,8	0,2	0,2	0,3	3,9	4,5	1,1	13
	CA008A	0,3	3,8	10,2	0,1	4,7	14	3,4	82	1,0	799,2	27,8	0,8	0,2	0,2	0,1	4,1	5,1	12	13
	CA008B	0,3	3,0	10,9	0,1	5,3	16	3,1	74	12	780,6	25,6	0,8	0,2	0,2	0,1	4,5	5,0	1,0	13
	CA012		4,5		14	11,1		12,2	448	18	599,4	8,0	0,9	0,1	0,2	14	20,0	10,9	0,7	2,3
	CA002A	10,2	5,4	340,6	0,8	3,9	39,9	1,9	17	2,8	656,6	11,6	0,5	1,0	0,1	0,8	6,6	29,9	1,1	1,5
	CA002B	15	5,0	52,2	2,8	6,0	9,1	6,8	112	18	443,0	9,8	0,7	0,3	0,2	2,8	7,9	17,0	0,9	2,1
	CA003	14	5,4	30,1	0,8	6,4	8,7	7,1	149	16	632,7	18,9	0,8	0,2	0,2	0,8	9,6	16,2	1,0	2,0
	CA004	0,1	3,8	4,9	0,0	8,1	0,6	1,6	107	0,9	1868,4	49,1	0,8	0,2	0,2	0,0	3,5	3,9	0,9	13
	CA005	0,5	3,6	17,3	12	4,0	2,2	4,7	60	14	517,1	19,1	0,7	0,3	0,2	12	3,4	5,9	0,8	13
	CA006	1,0	5,8	22,0	13	7,5	7,2	7,5	153	14	490,4	16,4	0,8	0,3	0,1	13	9,9	18,1	0,9	2,0
	CA007	0,2	3,2	6,1	0,8	7,5	13	1,3	43	0,9	635,7	29,9	0,7	0,3	0,2	0,8	4,7	7,4	0,9	14
	CA001A	0,2	3,4	6,2	15	7,2	16	1,1	35	3,6	618,7	29,4	0,7	0,3	0,2	15	5,5	10,0	0,8	18
	CA001B	0,4	2,8	15,2	0,1	12,9	4,5	5,0	129	2,7	619,1	20,7	0,7	0,4	0,1	0,1	8,9	19,2	0,9	14
	CA001C	0,3	3,4	13,4	0,2	5,4	18	2,8	72	0,4	610,7	21,9	0,9	0,4	0,2	0,2	3,8	7,6	0,9	14
	UCC	0,8	3,8	14,0	0,3	3,6	2,8	0,9	8	0,5	319,7	20,2	0,6	0,5	0,2	0,3	3,2	9,2	1,1	14

Alternative link

https://agrocienciauruguay.uy/index.php/agrociencia/article/view/525/1146 (pdf)